Electronic Supplementary Material (ESI) for Physical Chemistry Chemical Physics.
This journal is © the Owner Societies 2014

Supporting Information for

Compressibility, thermal expansion coefficient and heat capacity of CH_4 and CO_2 hydrate mixtures using molecular dynamics simulations

F.L. Ning [a], K. Glavatskiy[b], Z. Ji[c], S. Kjelstrup[d,e*], T. J. H. Vlugt[e]

[a] Faculty of Engineering, China University of Geosciences, Wuhan, Hubei, 430074, China.
[b] School of Applied Sciences, RMIT University, Melbourne VIC 3001, Australia.
[c] Faculty of Materials Science and Chemistry, China University of Geosciences, Wuhan, Hubei, 430074, China.
[d] Department of Chemistry, Norwegian University of Science and Technology, 7491- Trondheim, , Norway.
[e] Process & Energy Laboratory, Delft University of Technology, Leeghwaterstraat 39, 2628CB, Delft, The Netherlands.

1. Calculation of gas hydrates

1.1 The interaction potentials of molecules

There are three types of molecules in this study: CH_4, CO_2 and H_2O; therefore, the interaction potentials should capture the H_2O-H_2O, CH_4-CH_4, CO_2-CO_2, H_2O-CH_4, H_2O-CO_2 and CH_4-CO_2 interactions. The intermolecular interaction potential used in this study is a Lennard-Jones (LJ) site-site potential plus Coulombic interactions. The standard Lorentz-Berthelot rules, $\varepsilon_{ij}=(\varepsilon_{ii}\varepsilon_{jj})^{1/2}$ and $\sigma_{ij}=(\sigma_{ii}+\sigma_{jj})/2$, were used to derive the LJ potential parameters between unlike atom-types. ε_{ij} and σ_{ij} are the energetic and size parameters of the LJ interaction between sites i and j, respectively[1].

1.1.1 Host-host interaction water models. Many different water models have been used in molecular simulations. These models can be classified by the number of points used to define the model (atoms plus dummy sites), whether the structure is rigid or flexible, and whether the model includes polarisation effects. The water model selected eventually depends on the application. Most cases of gas hydrate simulations have used SPC/E and 4-site water potentials. These models are rigid and non-polarisable. The simple 3-site SPC model[2] for the water-water potential was used in the first MD simulation on gas hydrate[3]. Later, the SPC/E[4], TIP3P and TIP4P[5], TIP4PEw[6], TIP4PIce[7], TIP4P2005[8], TIP5P[9] and TIP5PEw[10] models were used[11-16], and a 6-site water model was also used[17-18]. We tested the eight mentioned models, which are all rigid models. Table S1 provides a comparison of the force field parameters. The polarisable water models are more successful at reproducing experimental data than are rigid models[19-21]; however, the computer time needed to use them becomes unreasonably large. This disadvantage restricted our selection to these rigid models.

The eight popular rigid water models selected here to describe the water-water interactions all contain a LJ potential for the oxygen-oxygen interactions and a Coulombic term for the electrostatic interactions between all charged sites. SPC/E and TIP3P are 3-site models that have three interaction sites, corresponding to the three atoms of the water molecule. Each atom is assigned a point charge, and the oxygen atom has LJ interactions. The 3-site models are popular in MD simulations because of their simplicity and computational efficiency. These models result in larger differences with the thermodynamic properties of water observed in experiments[8]. TIP4P, TIP4PEw, TIP 4PIce and TIP 2005 are 4-site models, in which a dummy atom is placed near the oxygen along the bisector of the HOH angle, which improves the charge distribution around the water molecule. Compared with the 3-site models, the 4-site models can provide reasonable structural and thermodynamic descriptions of liquid water[5]. TIP4P is often used for the simulation of biomolecular systems, and the TIP4PEw model is a reparameterisation of TIP4P for use with Ewald sums and provides an overall global improvement in water properties compared with the TIP4P model[6]. TIP4PIce can yield an excellent melting temperature of hexagonal ice I_h at 1 bar[7]. TIP4P2005 provides excellent performance for most of the water properties investigated, and the departures from the experiment for other properties are well balanced and justified[8]. TIP5P can better reproduce the temperature of the maximum density of water, and the TIP5PEw model is a reparameterisation of TIP5P for use with the Ewald summation[9-10].

Table S1: Intermolecular potential parameters for the water models used in this study.

Model	ε/k (K)[a]	σ (Å)[b]	q^- (e)[c]	$Q^+(e)$[d]	l_{OH} (Å)[e]	∠HOH (°)[f]
SPCE[4]	78.200	3.166	−0.8476(qO)	0.4238(qH)	1.0000	109.47
TIP3P[5]	76.540	3.151	-0.834(qO)	0.417(qH)	0.9572	104.52
TIP4P[5]	78.000	3.154	-1.04(qM)	0.52(qH)	0.9572	104.52
TIP4Pew[6]	81.900	3.164	-1.04844(qM)	0.52422(qH)	0.9572	104.52
TIP4Pice[7]	106.100	3.167	-1.1794(qM)	0.5897(qH)	0.9572	104.52
TIP4P2005[8]	93.200	3.159	-1.1128(qM)	0.5564(qH)	0.9572	104.52
TIP5P[9]	80.515	3.120	-0.241(qL)	0.241(qH)	0.9572	104.52
TIP5Pew[10]	89.573	3.097	-0.241(qL)	0.241(qH)	0.9572	104.52

[a] ε/k_B is the energy parameter of the LJ potential.

[b] σ is the size parameter of the LJ potential.

[c] q^- (e) is the negative charge, which is placed on the oxygen atom for the 3-site models (qO), or a dummy atom labelled M (qM) for the 4-site models and/or two dummy atoms labelled L (qL) for the 5-site models. The two dummy atoms represent the lone pairs of the oxygen atom and are located in a perpendicular plane to the HOH plane, forming an angle of ∠qOq= 109.5° and a O-q distance of l_{oq}= 0.7 Å.

[d] $Q^+(e)$ is the positive charge placed on the two hydrogen atoms (qH).

[e] l_{OH} is the O-H bond length.

[f] ∠*HOH* is the HOH bond angle.

1.1.2 Guest-guest interaction CH_4 and CO_2 potentials. For guest-guest interactions, several models have been proposed for the LJ potential for CH_4. The simplest is a single-site LJ potential[3]. A united-atom carbon-centred LJ potential based on optimised potentials for a liquid simulation (OPLS-UA) force field[22] has been used in many hydrate simulations[20-21,23-26]. Later, a united-atom potential for CH_4 was proposed by Goodbody et al[27] and used in the MD simulations of gas hydrate nucleation[12]. In fact, the CH_4 potential by Goodbody et al. and the TraPPE force field for CH_4 have almost the same values of potential parameters compared with the OPLS-UA potential for CH_4. Tse *et al.* first introduced a single-site LJ potential[3] and later a five-site rigid potential (also called TKM-AA)[28] for CH_4 with a C–H bond length of 1.094 Å in which electrostatic charges are assigned to all atoms but carbon is considered to be the sole interaction centre for LJ interactions[29]. This potential was adopted in several MD simulations of gas hydrate stability, formation and dissociation[28-30]. Other five-site LJ potentials for CH_4 are the Williams potential[31] and the Murad and Gubbins potential[32]. In this work, we employed the OPLS-UA potential and the DACNIS united-atom (DACNIS-UA) CH_4 potential for alkanes in nanoporous materials proposed by Martin et al.[33] to achieve relatively rapid calculations. We simultaneously adopted the full-atom TKM-AA potential for comparison. The rigid three-site TraPPE[34], EPM and EPM2 potentials[35] were selected for CO_2. The values of the parameters for the three CH_4 and CO_2 intermolecular potentials are listed in Table S2.

Table S2: LJ interaction parameters and partial charges for CH_4 and CO_2 molecules.

Model	Atom	ε/k (K)	σ (Å)	q (e) [a]
OPLS-UA[22]	CH_4	147.947	3.730	0
DACNIS-UA[33]	CH_4	158.500	3.720	0
TKM-AA[28]	C (CH_4)	164.172	3.640	-0.560
	H (CH_4)	0.000	0.000	+0.140
CCCTraPPE[34]	C (CO_2)	27.000	2.800	+0.700
	O (CO_2)	79.000	3.050	- 0.350
EPM[35]	C (CO_2)	28.999	2.785	+0.6645
	O (CO_2)	82.997	3.064	- 0.33225
EPM2 [35]	C (CO_2)	28.129	2.757	+0.6512
	O (CO_2)	80.507	3.033	- 0.3256

[a] q (e) is the positive or negative charge that is placed on the corresponding atom of the CH_4 and CO_2 molecule

The TKM-AA is an all-atom potential that places partial charges on the CH_4 atoms to reproduce the experimental gas phase octopole moment of CH_4 and assigns a LJ potential to the central carbon of CH_4 and no LJ interactions to the hydrogen atoms. The TraPPE CO_2 force field has three Lennard-Jones sites that model the overlap and dispersion interactions. Partial point charges are centred at each LJ site to approximate the first-order electrostatic and second-order induction interactions[36]. These two all-atom potentials for guest-guest interactions are both based on a rigid geometry. In MD simulations with the TKM-AA model, the bond lengths and angles of CH_4 are constrained to their experimental values, *i.e.*,

the bond length is 1.09 Å, and the bond angle is 109.471°. With the TraPPE CO_2 potential, the C-O bond length and O-C-O bond angle are fixed at 1.149 Å and 180°, respectively. The SHAKE algorithm[37] was used to handle these constraints in the MD simulations.

1.2 Computational procedure

MD simulations were performed with the eight water models combined with the three CH_4 interaction potentials in order to evaluate the ability of the model pairs to predict stable sI CH_4 hydrates. These tests were performed at 271.15 K (-2 °C) and 5 MPa. For each pair of interaction potentials, we obtained the lattice parameters and configurational energy of the sI CH_4 hydrates as a function of time. The NPT ensemble simulations were run for 5 ns and were divided into blocks of 1 ns to assess the statistical errors using block averages. It was also verified whether or not a stable hydrate state was obtained by investigating the atomic RDFs. Here, the microstructure of the hydrate is mainly described by the host's RDF g_{OO}(r) and the guest's RDF g_{CC}(r), where O is the corresponding oxygen site and C denotes the guest's centre of mass, *i.e.*, the carbon site. The NVT ensemble simulations were performed to calculate RDFs for system configurations before and after the NPT simulations. The NVT ensemble simulations were performed for a total time of 1 ns, with 0.5 ns used for temperature-scaled equilibration. The calculated results showed RDF shapes which were expected from experimental results and other MD simulations, except for the case of TIP3P. The first two peaks of $g_{OO}(r)$ are at approximately 2.78 Å and 4.5 Å, indicating the existence of tetrahedral hydrogen-bonding structures of H_2O molecules in CH_4 hydrates (Figure S1). However, the peaks of $g_{OO}(r)$ in TIP3P are the typical case of water, and the peaks of $g_{CC}(r)$ are also different from the other seven water models, namely a 3 Å-length left-translation. All characteristics in the RDF of the TIP3P water model imply that the structure is not a hydrate but has the structure of a hydrate that has decomposed (Figure S2). These results reveal that, except for TIP3P, seven water models and three CH_4 potentials can each describe the corresponding hydrate structures under conditions of hydrate stability.

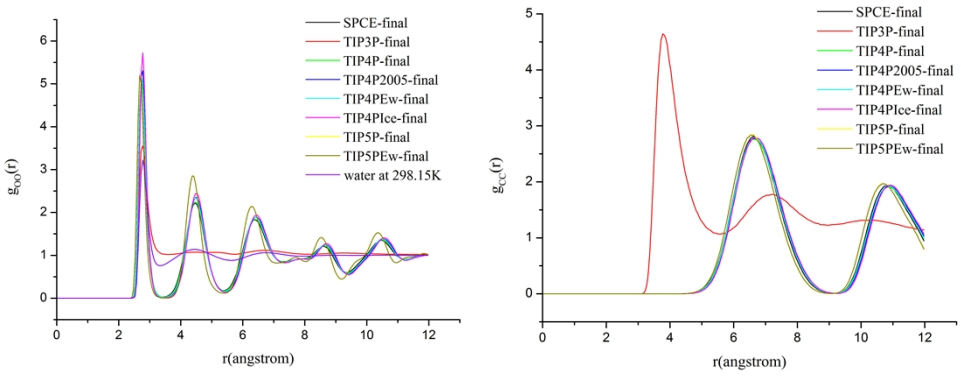

Figure S1: Radial distribution models goo(r) and gcc(r) of TKM five-site CH_4 hydrates with different water models (271.15 K and 5 MPa).

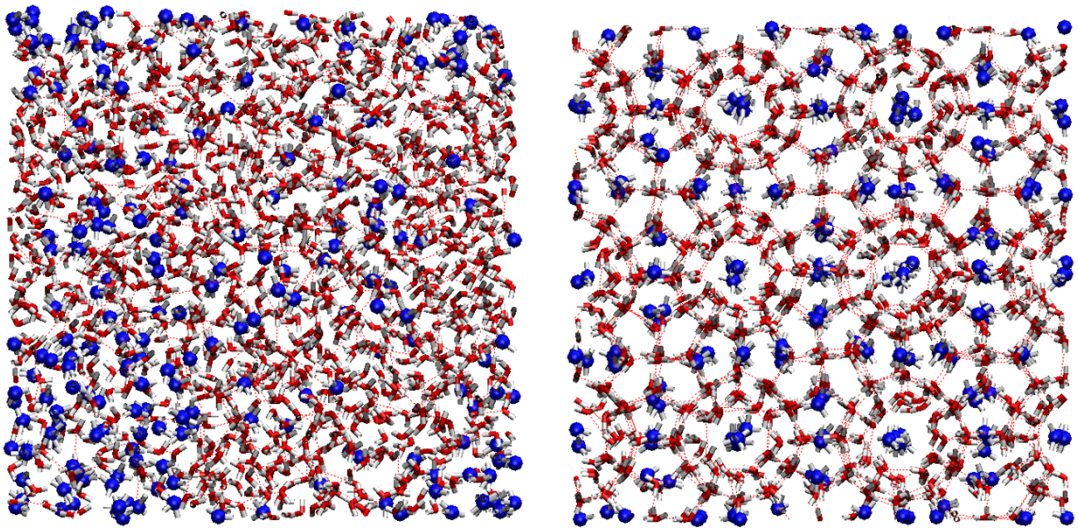

(a) (b)

Figure S2: snapshots of fully-occupied methane hydrates described by (a) TIP3P water model, where the methane hydrate decomposes at the end of the simulation; (b) TIP4P2005 water model, where the methane hydrate keeps stable.

1.3 Properties of gas hydrates calculated by the fluctuation method

The fluctuation method for calculation of compressibility, expansion and heat capacity of gas hydrates is derived from Ref. 38:

$$k_T = \frac{1}{k_B T \langle V \rangle}\left(\langle V^2 \rangle - \langle V \rangle^2\right)_{NPT} \tag{S1}$$

$$\alpha_P = \frac{\left[\langle V \cdot U \rangle - \langle V \rangle \cdot \langle U \rangle + P\left(\langle V^2 \rangle - \langle V \rangle^2\right)\right]_{NPT}}{k_B T^2 \langle V \rangle} \tag{S2}$$

$$C_P = \frac{ik_B N}{2} + \frac{1}{k_B T^2}\left[\begin{matrix}\left(\langle U^2 \rangle - \langle U \rangle^2\right) + \\ 2P\left(\langle V \cdot U \rangle - \langle V \rangle \cdot \langle U \rangle\right) \\ + P^2\left(\langle V^2 \rangle - \langle V \rangle^2\right)\end{matrix}\right]_{NPT} \tag{S3}$$

where k_T is the isothermal compressibility coefficient, Pa^{-1} T is the temperature, K; P is the pressure, MPa; V is the volume, $Å^3$; k_B is Boltzmann's constant and equal to 1.38×10^{-23} J/K; U is the potential energy, J; C_P is the heat capacity, J/K;. i is the number of degrees of freedom (DOF); and N is the number of molecules.

We adopted different simulation times and identified that the calculated properties do not change with time after 7 ns (Figure S3A). The thermal expansion coefficients at different temperatures and 20 MPa hardly change with time for simulations of 7 ns. Therefore, 7 ns was used as the final simulation time.

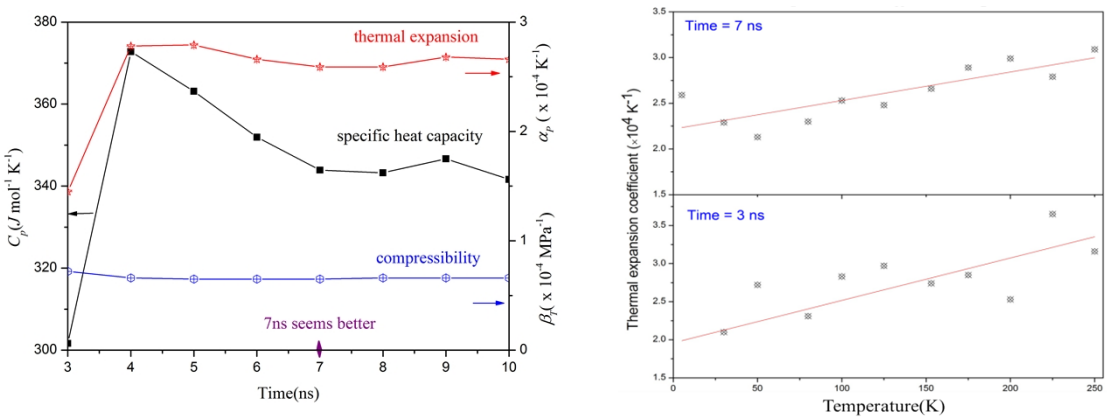

(a) (b)

Figure S3: (a) Computed thermodynamic properties as a function of the time of the MD simulation for 100% CO_2 at 20 MPa and 5K; (b) Thermal expansion coefficients at different temperatures and 20 MPa when simulation time was 3 ns (bottom) and 7 ns (top).

For calculation of the heat capacities of CH_4 and CO_2 hydrates via Eq. (S3), we observe that higher temperatures allow for a larger number of DOF of water molecules in hydrates. For example, at 271.15 K, i=3 results in a value of c_p closer to those reported in literature. However, at lower temperatures, i=0 is more suitable (Figures S4-5). Hydrate proton NMR analysis and dielectric constant measurements have suggested that at very low temperatures (<50 K), water molecular motion is "frozen in" so that hydrate lattices become rigid. The reorientation of water molecules is the first-order contribution to water motion in the structure; the second-order contribution is due to translational diffusion at these low temperatures. The rate of molecular water diffusion may be as much as two orders of magnitude slower in sI methane hydrate than in ice. This finding is one distinguishing feature differentiating between hydrates and ice[39].

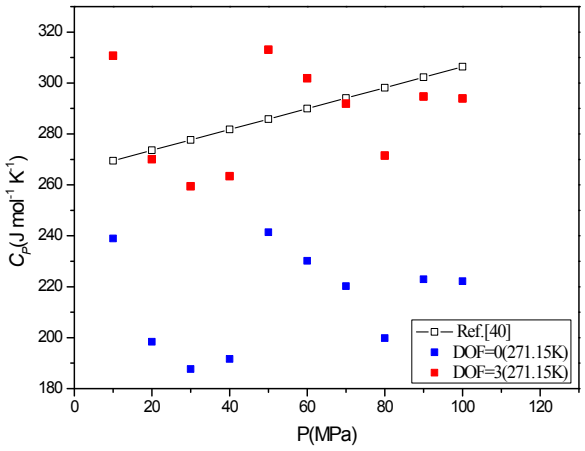

Figure S4: Pressure dependence of the specific heat capacity of fully occupied CH_4 at 271.15 K by using different degrees of freedom for the water molecule.

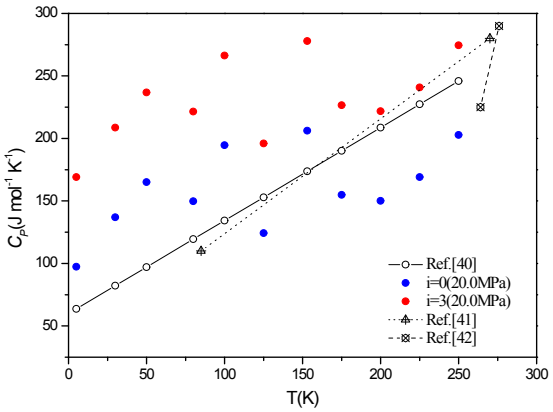

Figure S5: Temperature dependence of the specific heat capacity of fully occupied CH_4 at 20 MPa by using different degrees of freedom for the water molecule.

2. Calculation of liquid water

The first model for liquid water is a cubic box with cell length of 20.0 Å that contains 216 water molecules. The TIP4P/2005 and TIP5P water models were selected. Our simulation results show that the calculated density of 0.9972 g/cm^3 from the TIP4P/2005 water model is very close to the experimental value of 0.9970 g/cm^3[43] and the computed value of 0.9979 g/cm^3[44]. Therefore, we finally selected TIP4P/2005 as our water model and use its structure as our basic water structure. To consider the effect of periodic boundaries, we extended the system to a 2×2×2 supercell containing 1728 water molecules (Figure S6). The following computational parameters for this large system were used: cutoff= 12.0 Å, standard L-J potential for intermolecular interaction, P=0.1 MPa, T=298 K, NPT ensemble, rigid molecule, computation time=3 ns, equilibrium time=0.5 ns.

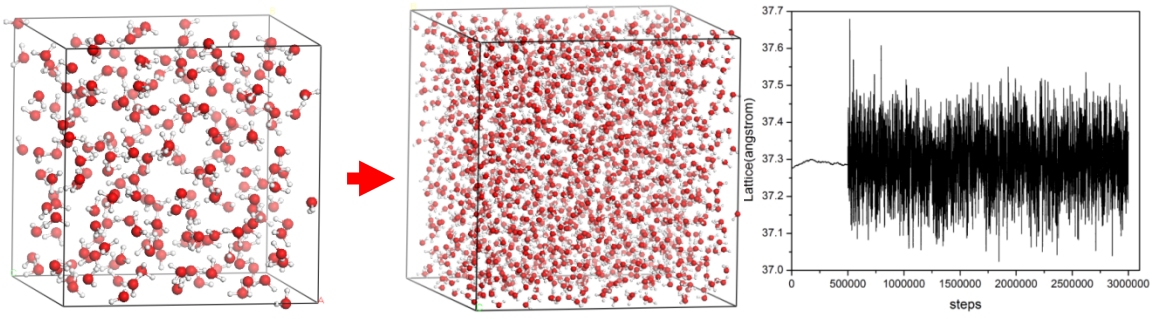

(a) Basic structure of liquid water (b) 2×2×2 supercell (c) Variation of lattice parameter after 0.5 ns equilibrium time. The average value is 37.2935 Å

Figure S6: Final structure and lattice of liquid water. The O and H atoms are colored red and white, respectively.

The calculated density of the system with 1728 water molecules is 0.9961 g/cm^3, which is close to

the experimental value of 0.9970 g/cm^3[43]. The RDFs are also similar to experimental results[43] (Figure S7).

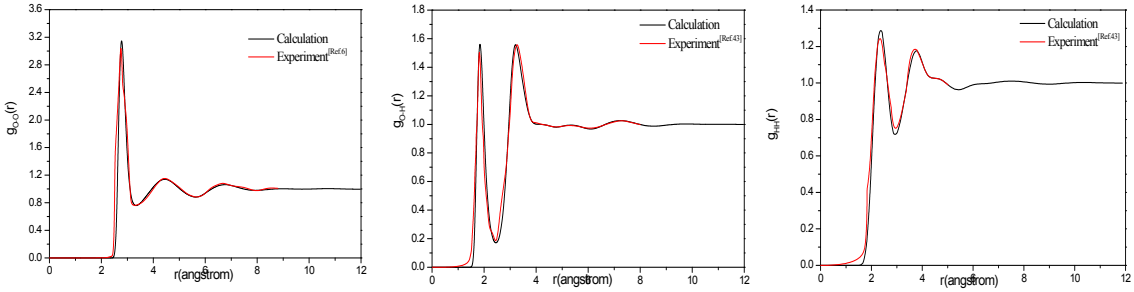

(a)O-O (b)O-H (c)H-H

Figure S7: calculation in this work and experimental RDFs of liquid water

Therefore, the simulated structure of liquid water is very close to the actual structure of liquid water. We used Eqs. (S1)-(S3) to calculate the compressibility, expansion coefficient, and heat capacity of liquid water, respectively. All our results are close to experimental or other calculated values (Table S3).

Table S3: Calculated and measured properties of liquid water.

Parameter	This work	Experiment [43]/calculation [44]
β_T (Pa^{-1})	4.64× 10^{-10}	4.58× 10^{-10}/4.65 × 10^{-10}
α_p (K^{-1})	2.25× 10^{-4}	2.57×10^{-4}/2.8 × 10^{-4}
c_p (J mol^{-1} K^{-1})	72.18(DOF=3)	72.0/75.6
	80.92(DOF=6)	81.6±2.8 [45-48]

3. Calculation of solid ice Ih

We further simulated solid ice I_h to reveal that the degree of freedom may be related to the phase of water molecules when heat capacity is calculated by the fluctuation method (Eq. (S3)).

The solid ice I_h model was a hexagonal box containing 96 water molecules (Figure S8). The water model TIP4P/2005 was selected. The following calculation parameters were used: NPT ensemble, rigid molecule, computation time=3 ns, equilibrium time=0.5 ns, cutoff= 5.0 Å, standard L-J potential, P=0.1 MPa, T=273.15K, 253.15K, 233.15K, 213.15K.

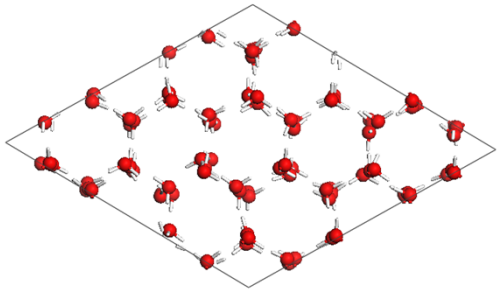

Figure S8: Structure of ice I_h. The O and H atoms are labelled in red and white, respectively.

The simulation results, including densities, structure, RDFs and heat capacity, are listed in Table S4.

Table S4: Calculated and measured densities of ice I_{hc}

Temperature (K)	213.15	233.15	253.15	273.15
Density(g/cm^{-3})-calculation	0.926	0.922	0.919	0.916
Density(g/cm^{-3})-experiment [49]	0.922	0.921	0.919	0.916

The calculated density of the system with 96 water molecules is close to the experimental value[50] (Table S4), as are the RDFs at the same conditions (Figure S9). Therefore, our structure of ice I_h is very close to the actual structure of ice Ih. Then, we used Eq. (S3) to calculate the heat capacity of ice I_h (i=0, 3, 6). The results are closer to the reported values[51] when the degree of freedom is lower (Figure S10). Although the data of c_p is scattered, but general trend is clear. Therefore, when using the fluctuation method to calculate the heat capacity of a water-related system, perhaps the temperature-related phase of the water molecules should be considered in order to reproduce results close to experimental values.

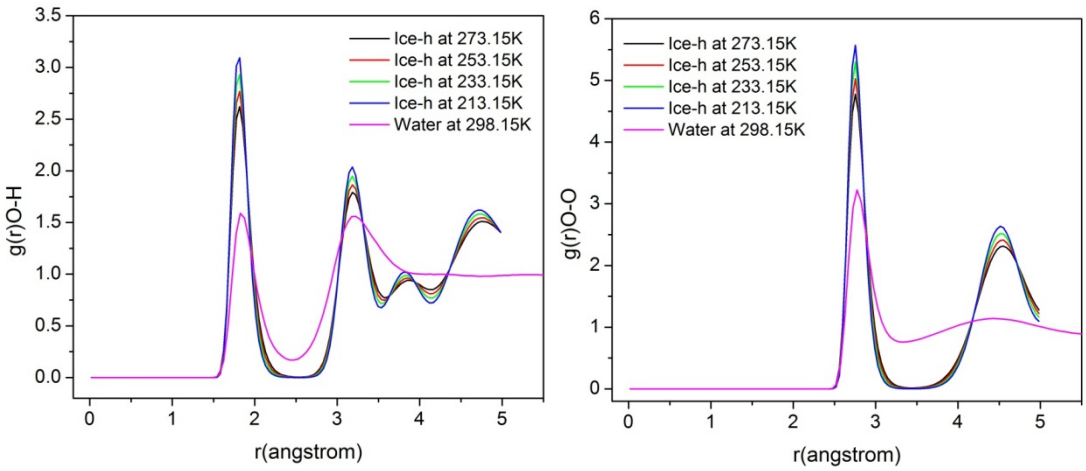

Figure S9: Calculated RDFs of ice I_h

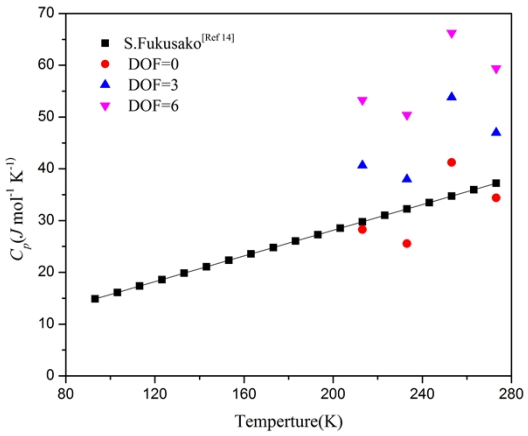

Figure S10: Calculated and reported heat capacity of ice I_h

References

1 J. S. Rowlinson, F. L. Swinton. Liquids and Liquid Mixtures, *Butterworth Scientific, London*, 1982.

2 H. J. C. Berendsen, J. P. M. Postma, W. Van Gunsteren, J. Hermans. Interaction models for water in relation to protein hydration, *Intermolecular forces*, 1981, **11**, 331-342.

3 S. T. John, M. L. Klein, I. R. McDonald. Dynamical properties of the structure I clathrate hydrate of xenon, *The Journal of chemical physics*, 1983, **78**, 2096-2097.

4 H. J. C. Berendsen, J. R. Grigera, T. P. Straatsma. The missing term in effective pair potentials, *Journal of Physical Chemistry*, 1987, **91**, 6269-6271.

5 W. L. Jorgensen, J. Chandrasekhar, J. D. Madura, R. W. Impey, M. L. Klein. Comparison of simple potential functions for simulating liquid water, *The Journal of Chemical Physics*, 1983, **79**, 926.

6 H. W. Horn, W. C. Swope, J. W. Pitera, J. D. Madura, T. J. Dick, G. L. Hura, T. Head-Gordon. Development of an improved four-site water model for biomolecular simulations: TIP4P-Ew, *The Journal of Chemical Physics*, 2004, **120**, 9665.

7 J. L. F. Abascal, E. Sanz, R. G. Fernández, C. Vega. A potential model for the study of ices and amorphous water: TIP4P/Ice, *The Journal of Chemical Physics*, 2005, **122**, 234511.

8 J. L. F. Abascal, C. Vega. A general purpose model for the condensed phases of water: TIP4P/2005, *The Journal of Chemical Physics*, 2005, **123**, 234505.

9 M. W. Mahoney, W. L. Jorgensen. A five-site model for liquid water and the reproduction of the density anomaly by rigid, nonpolarizable potential functions, *The Journal of chemical physics*, 2000, **112**, 8910.

10 S. W. Rick. A reoptimization of the five-site water potential (TIP5P) for use with Ewald sums. The Journal of Chemical Physics 2004, **120**, 6085.

11 E. J. Rosenbaum, N. J. English, J. K. Johnson, D. W. Shaw, R. P. Warzinski. Thermal conductivity of methane hydrate from experiment and molecular simulation, *The Journal of Physical Chemistry B*, 2007, **111**, 13194-13205.

12 M. R. Walsh, C. A. Koh, E. D. Sloan, A. K. Sum, D. T. Wu. Microsecond simulations of spontaneous methane hydrate nucleation and growth, *Science*, 2009, **326**, 1095-1098.

13 P. M. Rodger. Stability of gas hydrates, *Journal of Physical Chemistry*, 1990, **94**, 6080-6089.

14 H. Tanaka, K. Kiyohara. The thermodynamic stability of clathrate hydrate. II. Simultaneous occupation of larger and smaller cages, *The Journal of Chemical Physics*, 1993, **98**, 8110.

15 T. J. Frankcombe, G. J. Kroes. Molecular dynamics simulations of Type-sII hydrogen clathrate hydrate close to equilibrium conditions, *The Journal of Physical Chemistry C*, 2007, **111**, 13044-13052.

16 G. A. Tribello, B. Slater. A theoretical examination of known and hypothetical clathrate hydrate materials, *The Journal of Chemical Physics*, 2009, **131**, 024703.

17 H. Nada, J. P. van der Eerden. An intermolecular potential model for the simulation of ice and water near the melting point: A six-site model of HO, *The Journal of Chemical Physics*, 2003, **118**, 7401.

18 H. Nada. Growth mechanism of a gas clathrate hydrate from a dilute aqueous gas solution: A molecular dynamics simulation of a three-phase system, *The Journal of Physical Chemistry B*, 2006, **110**, 16526-16534.

19 H. Jiang, E. M. Myshakin, K. D. Jordan, R. P. Warzinski. Molecular dynamics simulations of the thermal conductivity of methane hydrate, *The Journal of Physical Chemistry B*, 2008, **112**, 10207-10216.
20 N. J. English, J. K. Johnson, C. E. Taylor. Molecular-dynamics simulations of methane hydrate dissociation, *The Journal of Chemical Physics*, 2005, **123**, 244503.
21 N. J. English, G. M. Phelan. Molecular dynamics study of thermal-driven methane hydrate dissociation, *The Journal of Chemical Physics*, 2009, **131**, 074704.
22 W. L. Jorgensen, J. D. Madura, C. J. Swenson. Optimized intermolecular potential functions for liquid hydrocarbons, *Journal of the American Chemical Society*, 1984, **106**, 6638-6646.
23 A. A. Chialvo, M. Houssa, P. T. Cummings. Molecular dynamics study of the structure and thermophysical properties of Model sI Clathrate hydrates, *The Journal of Physical Chemistry B*, 2002, **106**, 442-451.
24 G. J. Guo, Y. G. Zhang, H. Liu. Effect of methane adsorption on the lifetime of a dodecahedral water cluster immersed in liquid water: A molecular dynamics study on the hydrate nucleation mechanisms, *The Journal of Physical Chemistry C*, 2007, **111**, 2595-2606.
25 G. J. Guo, Y. G. Zhang, M. Li, C. H. Wu. Can the dodecahedral water cluster naturally form in methane aqueous solutions? A molecular dynamics study on the hydrate nucleation mechanisms, *The Journal of Chemical Physics*, 2008, **128**, 194504-194508.
26 B. Kvamme, T. Kuznetsova, K. Aasoldsen. Molecular dynamics simulations for selection of kinetic hydrate inhibitors, *Journal of Molecular Graphics and Modelling*, 2005, **23**, 524-536.
27 S. J. Goodbody, K. Watanabe, D. MacGowan, J. P. Walton, N. Quirke. Molecular simulation of methane and butane in silicalite, *Journal of the Chemical Society, Faraday Transactions*, 1991, **87**, 1951-1958.
28 S. T. John, M. L. Klein, I. R. McDonald. Computer simulation studies of the structure I clathrate hydrates of methane, tetrafluoromethane, cyclopropane, and ethylene oxide, *The Journal of Chemical Physics*, 1984, **81**, 6146-6153.
29 S. Alavi, J. A. Ripmeester, D. D. Klug. Molecular dynamics study of the stability of methane structure H clathrate hydrates, *The Journal of Chemical Physics*, 2007, **126**, 124708.
30 C. Moon, R. Hawtin, P. M. Rodger. Nucleation and control of clathrate hydrates: insights from simulation, *Faraday discussions*, 2007, **136**, 367-382.
31 D. E. Williams. Nonbonded potential parameters derived from crystalline hydrocarbons, *The Journal of Chemical Physics*, 1967, **47**, 4680.
32 S. Murad, K. E. Gubbins, P. Lykos. Computer modeling of matter. *In ACS Symposium. Series*, 1978, **86**, 62.
33 M. G. Martin, A. P. Thompson, T. M. Nenoff. Effect of pressure, membrane thickness, and placement of control volumes on the flux of methane through thin silicalite membranes: A dual control volume grand canonical molecular dynamics study, *The Journal of Chemical Physics*, 2001, **114**, 7174-7181.
34 J. J. Potoff, J. I. Siepmann. Vapor–liquid equilibria of mixtures containing alkanes, carbon dioxide, and nitrogen, *AIChE journal*, 2001, **47**, 1676-1682.
35 J. G. Harris, K. H. Yung. Carbon dioxide's liquid-vapor coexistence curve and critical properties as predicted by a simple molecular model, *The Journal of Physical Chemistry*, 1995, **99**, 12021-12024.
36 G. C. Maitland, M. Rigby, E. B. Smith, W. A. Wakeham. Intermolecular forces: their origin and determination, *Clarendon Press Oxford*, 1981.
37 J. P. Ryckaert, G. Ciccotti, H. J. Berendsen. Numerical integration of the cartesian equations of motion of a system with constraints: molecular dynamics of n-alkanes, *Journal of Computational Physics*, 1977, **23**, 327-341.
38 M. P. Allen, D. J. Tildesley. Computer simulation of liquids, *Oxford university press*, 1989.
39 E. D. Sloan, C. A. Koh. Clathrate hydrates of natural gases, *Taylor & Francis/CRC Press, Boca Raton, Florida*, 2008.
40 W. F. Waite, L.A. Stern, S.H. Kirby, W. J. Winters, D. H. Mason. Simultaneous determination of thermal conductivity, thermal diffusivity and specific heat in sI methane hydrate, *Geophysical Journal International*, 2007, **169**, 767-774.
41 Y. P. Handa. Compositions, enthalpies of dissociation, and heat capacities in the range 85 to 270K for clathrate hydrates of methane, ethane, and propane, and enthalpy of dissociation of isobutane hydrate, as determined by a heat-flow calorimeter. *The Journal of Chemical Thermodynamics*, 1986, **8**, 915-921.
42 R. Nakagawa, A. Hachikubo, H. Shoji. Dissociation and specific heats of gas hydrates under submarine and sublacustrine environments, *Proceedings of the 6th International Conference on Gas Hydrates*, 2008.
43 W. L. Jorgensen, J. Chandrasekhar, J. D. Madura, R. W. Impey, and M. L. Klein. Comparison of simple potential

functions for simulating liquid water, *The Journal of Chemical Physics*, 1983, **79**, 926.
44 J.L.Abascal, C.Vega. A general purpose model for the condensed phases of water: TIP4P/2005, *The Journal of Chemical Physics*, 2005, **123**, 234505.
45 M. W. Mahoney, W.L. Jorgensen. A five-site model for liquid water and the reproduction of the density anomaly by rigid, nonpolarizable potential functions, *The Journal of Chemical Physics*, 2000, **112**, 8910.
46 W.L.Jorgensen, C. Jenson. Temperature dependence of TIP3P, SPC, and TIP4P Water from NPT Monte Carlo Simulations: Seeking Temperatures of Maximum Density, *Journal of Computational Chemistry*, 1998, **19**, 1179-1186.
47 W.L.Jorgensen, Convergence of Monte Carlo simulations of Liquid water in the NPT ensemble, *Chemical Physics Letters*, 1982, **92**, 405-410.
48 P.v.R. Schleyer. Encyclopedia of Computational Chemistry British Library Cataloguing in Publication Data, 1998.
49 https://www.uwgb.edu/dutchs/Petrology/Ice%20Structure.HTM; http://www.physicsofmatter.com/NotTheBook/Talks/Ice/Ice.html; http://www.engineeringtoolbox.com/ice-thermal-properties-d_576.html; http://www1.lsbu.ac.uk/water/ice.html;http://hypertextbook.com/facts/2000/AlexDallas.shtml;http://www.its.caltech.edu/~atomic/snowcrystals/ice/ice.htm
50 M. Seidl, T. Loerting, G. Zifferer. High-density amorphous ice: Molecular dynamics simulations of the glass transition at 0.3 Gpa*, The Journal of Chemical Physics*, 2009, **131**, 114502.
51 S. Fukusako. Thermophysical properties of Ice Snow and Sea Ice, *International Journal of Thermophysics*, 1990, **11**, 353-372.